Korean J. Chem. Eng., 39(12), 3323-3333 (2022)
DOI: 10.1007/s11814-022-1206-0

pISSN: 0256-1115
eISSN: 1975-7220

A facile method for efficient synergistic oxidation of Fe^{2+} in phosphorus-sulfur mixed acid system with a mixture of oxygen and ozone

Dong-yan Liu*, Wen-bo Lou,***,†, Shi-neng Sun****, Yang Zhang***, Ying Zhang***, and Shi-li Zheng*****

*Normal College, Shenyang University, Shenyang 110044, China
**School of Metallurgy, Northeastern University, Shenyang 110819, China
***National Engineering Research Center of Green Recycling for Strategic Metal Resources, Chinese Academy of Sciences, Institute of Process Engineering, Beijing 100190, China
****Institute of Innovative Science and Technology, Shenyang University, Shenyang 110044, China
(*Received 10 February 2022 • Revised 21 May 2022 • Accepted 12 June 2022*)

Abstract−The recovery of iron phosphate involves the addition of oxidizer to oxidize Fe^{2+} in the spent $LiFePO_4$ (LFP) material to Fe^{3+} and the agent commonly used is hydrogen peroxide (H_2O_2). Nevertheless, H_2O_2 has disadvantages of high price, easy decomposition and low utilization efficiency. In this manuscript, a facile method is proposed for efficient synergistic oxidation of Fe^{2+} in spent LFP leachate with a mixture of oxygen and ozone. Specifically, we found by thermodynamic computations that the dominant oxidation groups of ozone during oxidation varied with acidity. The oxidation would produce a large number of iron-phosphate complex groups ($Fe_3H_6(PO_4)_4^{3+}$, $FeH_8(PO_4)_4^-$ and $Fe_2HPO_4^{4+}$) in the phosphorus-sulfur mixed acid system, leading to a paradoxical pH drop. The optimized conditions for H_2O_2 oxidation were explored. It was determined experimentally that oxidation by gas mixture and O_2 belonged to the first-order and second-order reactions with activation energies of 28.68 kJ/mol and 34.61 kJ/mol, respectively, which were both controlled by a mixture of chemical reaction and diffusion. The optimized oxidation method was finally determined by evaluating the cost and oxidation rate of the oxidizers. The results in this study offer a promising method for new low-cost and efficient Fe^{2+} oxidation for industrial production.

Keywords: Synergistic Oxidation, Mixed Acid System, Ozone, Oxygen, $LiFePO_4$ Leachate

INTRODUCTION

Since lithium iron phosphate ($LiFePO_4$, abbreviated as LFP) batteries were developed, they have received much attention for their high safety, low cost and long service life [1,2]. A number of policies have been released in China since 2009 to promote the development of new energy vehicle industry [3,4]; the number of vehicles with LFP power batteries as energy source has been increasing annually, from less than 5,000 in 2011 to 750,000 in 2017 [5]. After 5-8 years of service, there are nearly 700,000 tons of end-of-life LFP power batteries in the market, which urgently demand for safe disposal [6].

At present, it is believed that the optimum method for recycling is to scrap the spent batteries and then sort them by category [7]; the cathode, anode, separator, shell, electrolyte and other parts can be obtained individually [8]. In particular, the value of cathode powder can account for more than 33% of the whole battery, which is the chief target in the recycling process. For the spent LFP cathode powder, recycling can be roughly classified into physical rehabilitation [9] and chemical hydrometallurgical methods [10,11] based on the different treatment patterns. Physical method involves directed supplementation of the Li/Fe/P source into the spent LFP material, with subsequent ball milling and roasting essential. The electrochemical performance of the rehabilitated LFP powder can reach about 90% of that of commercial grade LFP powder, which is a significant improvement. Nevertheless, the rehabilitation process does not have the capacity to remove impurities and a relatively high purity of the raw material is required, which makes it narrowly applicable. In contrast, chemical hydrometallurgical methods do not require high purity of raw materials, as they involve leaching the spent LFP cathode powder with acid to obtain the solution containing Li^+, Fe^{2+} and PO_4^{3-}, adding oxidant to completely oxidize Fe^{2+} to Fe^{3+}, then preparing $FePO_4$ by neutralization/hydrothermal method, finally recycling Li with carbonate [12].

Moreover, besides LFP, there are other scrapped high-efficiency energy storage electrode materials [13-16], especially Li and post Li ion battery [17,18] electrode materials [3,4,7] such as $LiCoO_2$ [19], $LiNi_{0.5}Co_{0.2}Mn_{0.3}O_2$ [20], etc., can also be selectively extracted by hydrometallurgy [21,22] for Li element. Mechanically, it oxidizes Fe, Co, Ni and other variable elements while leaching the raw material in low concentration acid, forming acid-insoluble solids, distorting the original crystal lattice and de-embedding Li^+ into the solution.

The hydrometallurgical process includes leaching, separation, crystallization and other purification operations, which can effectively deal with various materials containing impurities with high overall utilization efficiency and is therefore considered a promising method for recycling spent LFP powder.

†To whom correspondence should be addressed.
E-mail: wbolou@163.com

At present, there are extensive studies on hydrometallurgical recovery processes for spent LFP cathode materials in the literature [23, 24]. The oxidation of leachate from spent LFP cathodes is generally performed with H_2O_2, which is characterized by fast reaction speed, non-polluting products and no introduction of any impurities. For practical applications, H_2O_2 is inevitably consumed during storage and transport due to its easily decomposable properties. Furthermore, the Fenton reaction caused by the addition of H_2O_2 can generate large amounts of Fe^{3+} rapidly, which in turn promotes the decomposition of H_2O_2, resulting in low utilization (60%-80%) [25] and high oxidation costs, and the industrial recovery of spent LFP cathode material by hydrometallurgy is impeded to some extent. Consequently, there is an urgent demand to establish a new low-cost and efficient oxidation method for Fe^{2+} in spent LFP leachate.

Industry-wide oxidants that do not introduce impurities, besides H_2O_2, are O_2, O_3 and their complexes, including O_3/Persulfate (PMS/PS) [26], O_3/UV photocatalytic [27], O_3/H_2O_2 [28], O_3/Fenton [29], O_3/Ultrasound (US) [30], O_3/electrochemistry [31], O_3/hydroxylamine (HA) [32], O_3/peroxynitrite [33], etc. Since O_2 in the ground state is a paramagnetic molecule in the trilinear state [34,35], which is relatively inert, the industrial application is mainly as a raw material for synthesis. Kawabata et al. [36] used benzaldehyde/sec-ol as the sacrificial agent and the peroxybenzoic acid was generated by O_2 oxidation of benzaldehyde in situ, which could be oxidized ketone into lactone compounds. Generally, some catalysts [36-39] of Fe_2O_3, Cu-MCM-41, hydrotalcite, $(NH_4)_2Ce(NO_3)_6$, etc. are introduced into the process to convert O_2 into O-containing active species to accelerate the reaction. Zhang et al. [40] prepared covalent triazine frameworks and investigated their reactions of catalyzing alcohol oxidation to aldehydes under O_2 conditions. It was found that, under light conditions or UV light irradiation [41], photogenerated electrons activated O_2 to $O_2^{-}\cdot$ with $^1O_2$, and $O_2^{-}\cdot$ combined with H atoms (benzyl alcohol) further converting to ·OOH, thereby facilitating the reaction. In comparison, O_3 has extremely strong oxidizing properties, with a redox potential of 2.07 V, which is only lower than that of fluorine atoms, oxygen atoms and hydroxyl radicals ($E_{OH\cdot}$= 2.8 V). It offers a much larger field of application [42], including oxidative synergistic leaching [43], oxidative disposal of solid waste [44] and decomposing the organic matter in wastewater [45], which is by far its most widespread aspect. Due to the high environmental impact on the solubility and stability of O_3 in water, there are difficulties of degrading persistent organics such as polycyclic aromatic hydrocarbons (PAHs) by O_3 molecules alone; it is often used along with catalysts. Bourgin et al. [46] determined that 12 micropollutants had an average removal efficiency of more than 80% and 550 substances had an average removal efficiency of more than 79% when O_3 was applied at 0.55 mg O_3/mg DOC. Jia et al. [47] observed that organics with molecular weights of 5-6 kDa and 1-3 kDa were significantly removed with the increase of ozone contact time and the removal efficiency was more than 50%. In fact, the results of O_3 treatment for COD in wastewater are closely related to factors such O_3 dosage and reaction time, while temperature and pH have minor effects on the treatment results.

For the Fe^{2+} oxidation in LFP solution, Tang et al. [48] attempted to oxidize Fe^{2+} in solution with air or O_2, the reaction temperature was up to 90-95 °C with high energy consumption and no detailed analysis was performed for the oxidation process. Wang et al. [49] simulated the leaching of spent LFP material with H_3PO_4 and used microbubble technology to strengthen oxidation. They found that the complete oxidation of Fe^{2+} could be achieved at these conditions: a temperature of 90 °C, a H_3PO_4 concentration of 30 wt% and a reaction time of 90 min with a 0.22 μm titanium aeration head; they confirmed that the reactive oxygen species (OH·) generated at the moment of microbubble bursting was the reason for the high oxidation activity of the system. In fact, H_2SO_4 is recognized as a reasonable industrial leaching agent in the recovery process for the low price, high acidity and low impact on the equipment, but the oxidation behavior of Fe^{2+} in phosphorus-sulfur mixed acid systems is rarely reported and the changes in ionic groups and system parameters during oxidation are often ignored, which may lead in turn to a modification of the whole LFP recovery process. Moreover, most of the current studies set the oxidation temperature over 90 °C, which is unfavorable for the actual green and environmentally friendly industrial recycling of spent LFP materials.

Therefore, in this manuscript a facile method for efficient synergistic oxidation of Fe^{2+} in phosphorus-sulfur mixed acid system with a mixture of O_2 and O_3 is proposed. The reactions of Fe^{2+} oxidation by H_2O_2, O_2 and O_3 were previously investigated, the oxidation pathways and mechanisms of the three oxidants in solution were reviewed and compared, and the complexation groups of Fe^{3+} and phosphoric acid during the oxidation process were computationally analyzed to theoretically determine the changes of pH value of the solution after the reaction. The oxidation effects and reaction kinetics of H_2O_2, O_2 and gas mixture (O_2 and O_3) were compared to determine the appropriate oxidation method from economy and timeliness.

EXPERIMENTS

1. Raw Materials and Reagents

The leachate to be oxidized in the experiment was leached from spent LFP powder with H_2SO_4 aqueous solution. There was 56 g/L iron (divalent) and 31 g/L phosphorus in the solution with pH 1.62.

The water used in the experiments was deionized water (Resistivity 18.2 MΩ·cm), which was purified by a Millipore purification system. Sodium diphenylamine sulfonate (≥97.00%), $K_2Cr_2O_7$ (≥99.95%), $FeSO_4{\cdot}7H_2O$ (≥99.95%), H_2O_2 (≥30.0%) and H_2SO_4 (≥98.00%) purchased from Aladdin Reagent Co., Ltd. were of analytical purity. High purity oxygen (99.995% purity) from HuanYu JingHui Co., Ltd. was used in oxidations.

2. Oxidation Process Description

For unified standards, the pH of all the solutions was adjusted to 1.30 with H_2SO_4 before oxidation, and the volume used was always 0.5 L.

The solution was put into a 1 L beaker. The beaker was placed in a water bath, which was a confined environment for recoverable gases. When the inner temperature reached the set temperature, the oxidants were added.

When the oxidant was H_2O_2, a peristaltic pump was used to adjust the adding rate and the oxidant was O_2/O_3; the gas tube with an aeration head was inserted into the bottom of the solution and the gas flow rate was adjusted with a gas flow meter. The effects of vari-

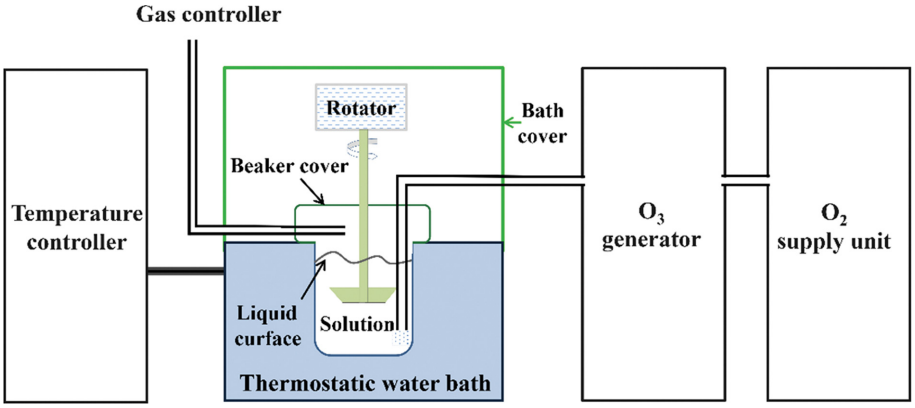

Fig. 1. Ozone oxidation experimental device.

ous factors and reaction kinetics on oxidation of solution were explored, including initial pH, temperature, oxidant adding rate. Note that the O_3 in the laboratory was prepared by an ozone generator (AYOY-5P2A, Beijing 322 Technology Co.) with a conversion efficiency of 10%, i.e., the gas produced contained 90% O_2 and 10% O_3, of which oxidation experimental device is shown in Fig. 1.

It should be highlighted that when different environmental systems were experimentally compared for oxidation effects, the experimental process was repeated through three times to confirm the reliability and reproducibility of the results, and the data were averaged for analysis.

3. Analysis Methods

For calculating the oxidation efficiency, the formula is given as follows:

$$X_i\% = \left(1 - \frac{V_i * C_i}{V_0 * C_{i0}}\right) * 100\%$$

where X_i is the oxidation efficiency at some time, V_0 and V_i are the volume of the initial solution and the solution at some time, respectively. C_i and C_{i0} are the content of ferrous iron at initial moment and some moment in the reaction.

Analysis content of ferrous iron: 0.001 L oxidized solution was taken into a 0.1 L Erlenmeyer flask, adding 0.02 L thiophosphorus mixed acid (volume ratio of 98% H_2SO_4 : 85% H_3PO_4 : H_2O=1.5 : 1.5 : 7) and 4 drops of sodium diphenylamine sulfonate indicator (5 g/L); the mixture was evenly mixed. $K_2Cr_2O_7$ standard titration solution (0.0500 mol/L) was used to titrate until the color of the solution was purple. It could be considered that the titration end point had been reached when the purple lasted for more than 30 s. Calculation formula is as follows:

$$C_{Fe^{2+}} = C * \frac{(V - V_0)}{0.001} * 55.85$$

where $C_{Fe^{2+}}$ is content of ferrous iron g/L, C is actual concentration of $K_2Cr_2O_7$ standard titration solution mol/L, V and V_0 are volumes of $K_2Cr_2O_7$ standard titration solution consumed by titrating the oxidized solution and the blank solution L, 55.85 is molar mass of iron g/mol, 0.001 is volume of oxidized solution for testing L.

The concentration of elements in the solution was analyzed by inductively coupled plasma atomic emission spectrometry (Optima 5300DV, USA). Solution acidity was measured by a pH meter (FE28, Switzerland).

RESULTS AND DISCUSSION

1. Calculation of Δ_rG^o and Δ_rH^o in the Oxidation Process

Eq. (1)-Eq. (3) are the reaction equations of H_2O_2, O_2 and O_3 involved in the oxidation process. Curves of Δ_rH^o, Δ_rG^o with temperature are illustrated in Fig. 2(a) and 2(b). The results show that the Δ_rH^o are negative for all three and the variations are not significant in the range of 0-100 °C, which indicates that the oxidation process is exothermic. If the reaction is carried out according to the standard stoichiometry, the expected energy has the following order: O_3>O_2>H_2O_2. The Δ_rG^o are all negative and the value tends to increase gradually with elevated temperature, demonstrating that there are tendencies for the oxidation reaction to proceed spontaneously in all experimental temperatures.

$$H_2O_2 + 2H^+ + 2Fe^{2+} = 2Fe^{3+} + 2H_2O \quad (1)$$

$$O_2 + 4H^+ + 4Fe^{2+} = 4Fe^{3+} + 2H_2O \quad (2)$$

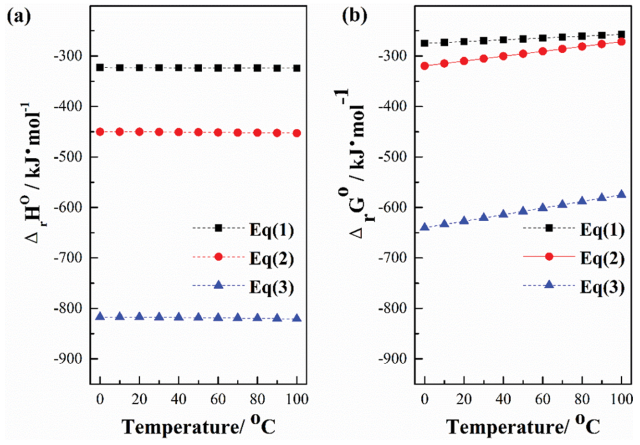

Fig. 2. The relationship between (a) Δ_rH^o, (b) Δ_rG^o and temperature of Eq. (1)-(3).

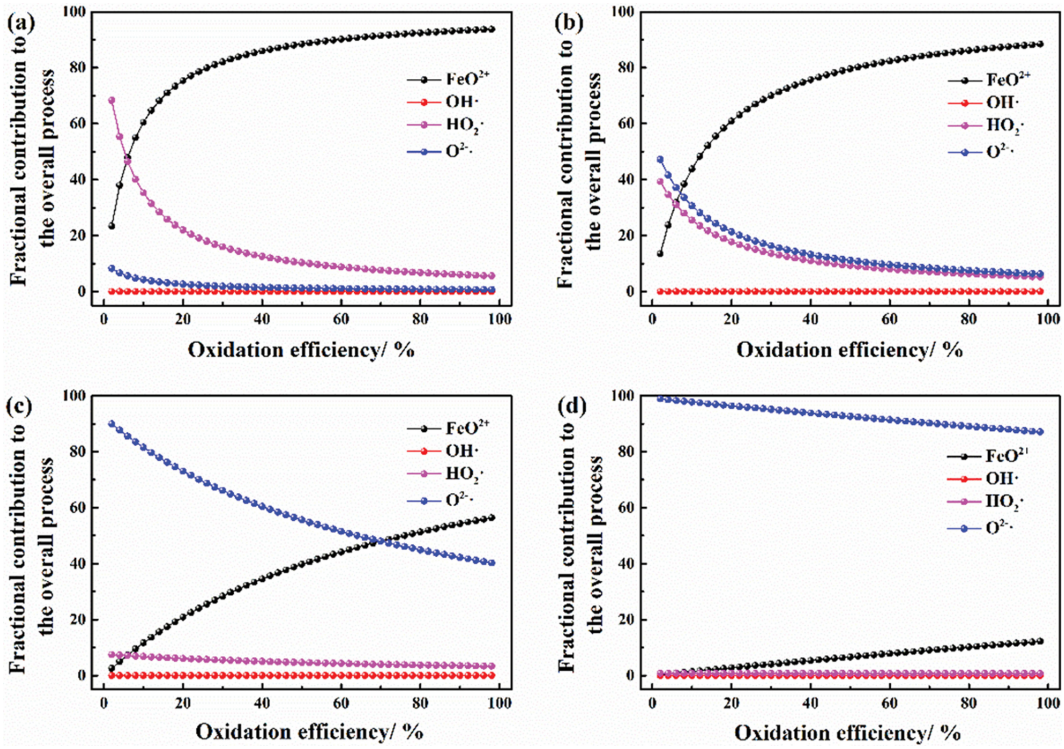

Fig. 3. The change of contribution rate of main oxidizing groups in the oxidation process under different constant C_{H^+} ((a)-(d): 1.0 mol/L, 0.1 mol/L, 0.01 mol/L and 0.001 mol/L).

$$O_3+6H^++6Fe^{2+}=6Fe^{3+}+3H_2O \quad (3)$$

2. The Oxidation Pathway at Different Acidity

The oxidation mechanism of the three oxidants mentioned is similar, which is releasing the highly oxidative ionic/radical groups during the reaction. The main oxidative groups include FeO^{2+} active intermediates, OH· hydroxyl radicals, HO_2· superoxide radicals and O_2^-· peroxyl radicals [50,51].

During the oxidation of O_2, various major oxidizing groups are produced at a slow rate due to the limitation of gas activity, while O_3 in the experiment is generated by bombarding oxygen molecules with electron beams, dissociating into atoms and combining with other oxygen molecules, which is unstable and strongly oxidizing. After feeding into the solution, dissolved O_3 can rapidly form FeO^{2+} with Fe^{2+}, while causing a series of other chain reaction processes, the specific reaction process is shown in supplementary Table S1 (refer to online supplementary material) [52,53]. FeO^{2+}/O_3^- intermediate is produced first. Then, by binding with H_2O or H^+, OH·, HO_2· and O_2^-· groups are subsequently generated to advance the reaction rapidly. When H_2O_2 is added to the leachate, H_2O_2 reacts with Fe^{2+} therein via the Fenton reaction, the main mechanism is shown in supplementary Table S1 as reaction number 17. Fe^{2+} can be regarded as the catalyst of the reaction and its concentration is proportional to the reaction rate; a large amount of extremely oxidizing OH· is produced in the process, which is the main oxidizing group.

In this subsection, the changes in the proportion of the contribution of each major acting group to the O_3 oxidation of Fe^{2+} are used to analyze the process involved. As a simplified analysis, the reactions of FeO^{2+}, OH·, HO_2· and O_2^-· directly applying to Fe^{2+} at constant acidity are taken as the basis for the evaluation. From the rate constants of each reaction in supplementary Table S1 (the inverse reactions are neglected and the forward reaction rate constant is chosen as the equilibrium constant), the concentration of each group is determined, combining further with the coefficients that contribute to the oxidation capacity, the proportion of each component in the process is identified, which is illustrated in Fig. 3(a)-(d). The results reveal that the oxidizing groups are mainly dominated by FeO^{2+} when the acidity is high (C_{H^+}>0.10 mol/L) and the proportion of their contribution became progressively larger as the reaction proceeded. Since FeO^{2+} is primarily developed as an intermediate through the direct combination of O_3 and Fe^{2+}, indicating that the O_3 oxidation process under high acidity is roughly based on the production of FeO^{2+} first and then the reaction with Fe^{2+} to obtain Fe^{3+}. When the acidity decreases (C_{H^+}<0.01 mol/L), it is dominated by O_2^-·, the generation of which consumes OH^- and is inhibited at high acidity.

3. Drop in pH of Mixed Acid System after Oxidation

To determine the effect of phosphate groups on the oxidation process more intuitively, the following experiments were designed. The oxidation effect of a single sulfuric acid system simulation solution (consisting of $FeSO_4{\cdot}7H_2O$, Li_2SO_4, $Al_2(SO_4)_3$, H_2SO_4 and H_2O), under the same oxidation conditions (H_2O_2 as oxidant, adding rate 1.5 mL/min, temperature 25 °C, stirring rate 400 rpm), was compared with that of the phosphorus-sulfur mixed acid system and the specific parameter differences between the two are listed in supplementary Table S2.

As stated in the "Oxidation process description" section, this part

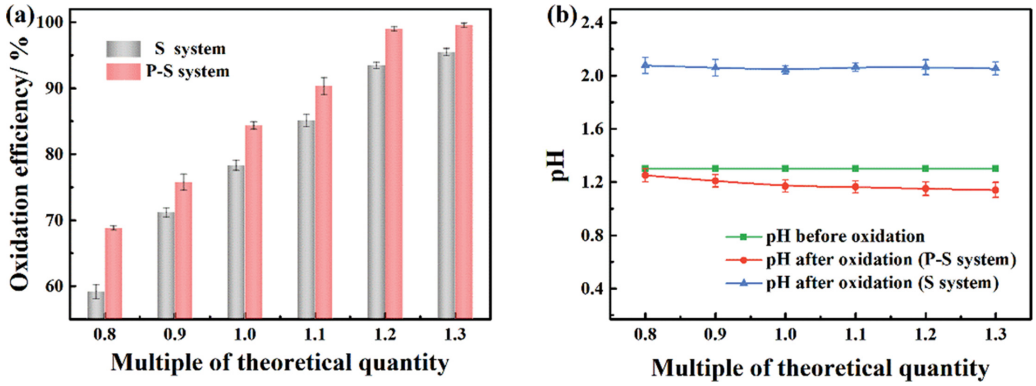

Fig. 4. (a) Comparison of the oxidation effect of the leaching solution and the simulated solution at different H_2O_2 dosage (b) Comparison of pH value before and after oxidation.

of the experiment was performed in several replications and some differences can be clearly identified. The comparison results are illustrated in Fig. 4(a), which shows the oxidation efficiency of both with different doses of H_2O_2 added. It can be clearly observed that both of them have a rapid increase in oxidation efficiency with higher amount, except that the oxidation efficiency of phosphorus-sulfur mixed acid system is always about 8% higher than that of single sulfuric acid system. Fig. 4(b) presents the changes of pH before and after oxidation; the pH was 1.30 before oxidation, but after oxidation, the pH of the single sulfuric acid system increased and the pH of the phosphorus-sulfur mixed acid system decreased, which is a very obvious contrasting trend.

The pH of the leach solution was in the range of 0 to 2 throughout the experiment. According to the phosphate distribution equation, the phosphorus-sulfur mixed acid system of the leach solution before oxidation contains a large number (>90%) of phosphate molecules [54]. The complexation of phosphate molecules is through the coordination of metal ions by oxygen on the phosphate, which is particularly suitable for coordination with high valent (above +3) metal ions. After oxidation, significant amounts of trivalent iron ions are rapidly produced in the system, which gradually complex with phosphoric acid molecules. After the preliminary thermodynamic calculations of our group [55], the main complexes are considered to be $Fe_3H_6(PO_4)_4^{3+}$, $FeH_8(PO_4)_4^-$ and $Fe_2HPO_4^{4+}$. For each 1 M of complex produced, the system releases 2 M, 4 M and 1 M of H^+, respectively, leading to a drop in pH after oxidation. On the other hand, since the trivalent iron is complexed and the catalytic decomposition of H_2O_2 is reduced, the presence of the phosphate

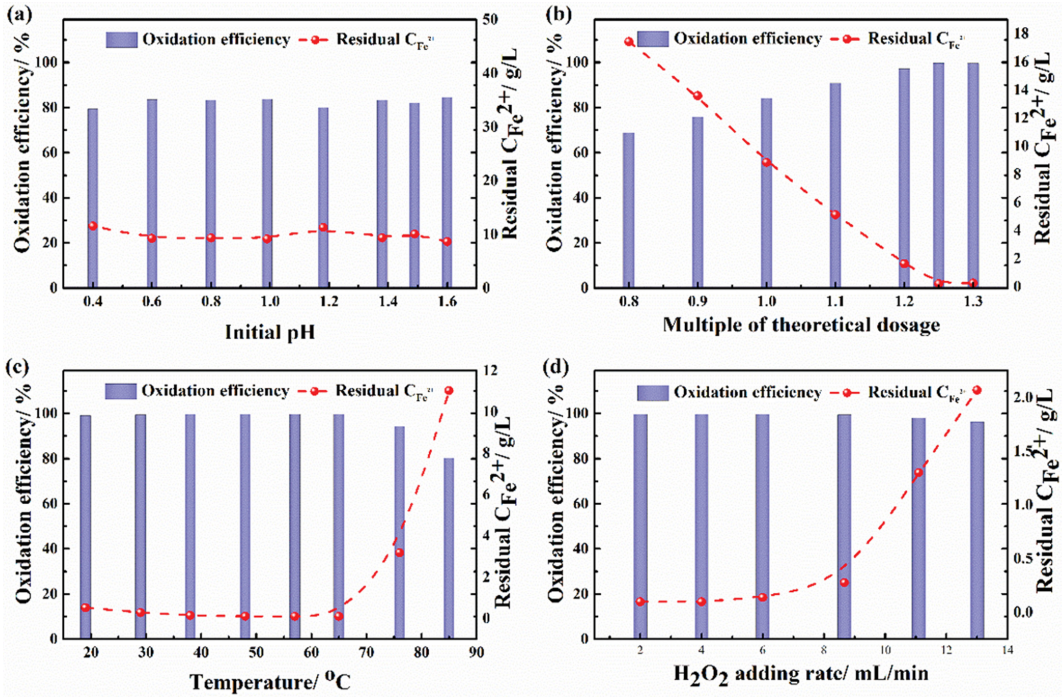

Fig. 5. Effects of various factors on oxidation efficiency and residual $C_{Fe^{2+}}$ ((a)-(d): initial pH, multiple of theoretical consumption, temperature, H_2O_2 adding rate).

group can facilitate the oxidation reaction to some extent.

4. Optimized Conditions for H_2O_2 Oxidation

The effect of initial pH on the oxidation efficiency and residual $C_{Fe^{2+}}$ is illustrated in Fig. 5(a). The specific experimental conditions are: a H_2O_2 addition rate of 1.5 mL/min, a dosage of 1.0 times the theoretical amount, a reaction time of 30 min and a temperature of 20 °C. The initial pH ranges from 0.4 to 1.6, the oxidation efficiency is stabilized at 82% and the residual $C_{Fe^{2+}}$ is about 10 g/L. The above results indicate that the initial C_{H^+} in the solution has no significant effect on the oxidation process.

The effect of H_2O_2 addition on the oxidation efficiency and residual $C_{Fe^{2+}}$ is shown in Fig. 5(b). The experimental conditions are: a H_2O_2 addition rate of 1.5 mL/min, a reaction temperature of 20 °C, a reaction time of 30 min and an initial pH of 1.3. When the theoretical amount of H_2O_2 is added, the oxidation efficiency is about 83%. Increased to 1.25 times, the efficiency is over 99.9%. The oxidation product Fe^{3+} is a good catalyst for the decomposition of H_2O_2, leading to the waste of oxidant. Therefore, an excess amount of H_2O_2 is required for complete oxidation.

The effect of temperature is plotted in Fig. 5(c). The experimental conditions are a H_2O_2 addition rate of 1.5 mL/min, 1.25 times of the theoretical amount of H_2O_2, a reaction time of 30 min and an initial pH of 1.3. The results reveal that the effect of temperature is not significant below 65 °C. The elevated temperature causes the decomposition of H_2O_2 and a significant decrease in oxidation efficiency can be noticed. Fig. 5(d) exhibits the effect of H_2O_2 addition rate on oxidation efficiency and residual $C_{Fe^{2+}}$ (1.25 times the theoretical amount of H_2O_2, a temperature of 40 °C, a reaction time of 30 min and an initial pH 1.3). Similar to the effect of temperature, the H_2O_2 addition rate has almost no effect until 6 mL/min. When the rate is increased, the oxidation efficiency decreases sharply. According to the aforementioned thermodynamic analysis, the oxidation of Fe^{2+} by H_2O_2 is a massive exothermic reaction and the rapid addition of H_2O_2 leads to high local temperature, resulting in the decomposition of H_2O_2.

The optimized conditions for H_2O_2 oxidation are determined through experiments: the amount of H_2O_2 is 1.25 times of the theoretical amount, the rate of H_2O_2 addition is lower than 6 mL/min (corresponding to 500 mL leaching solution) and the oxidation temperature is lower than 65 °C. The oxidation efficiency of Fe^{2+} can reach more than 99.9% under this condition.

5. Kinetics of O_2 Oxidation Process

According to the theory of chemical reaction rate equations, Eq. (2) follows the law of mass action when the inverse reaction is not considered. There is usually an empirical rate Eq. (4):

$$r_{O_2} = -\frac{dC_{Fe^{2+}}}{dt} = kC_{Fe^{2+}}^{a} V_{O_2}^{b} C_{H^+}^{c} \quad (4)$$

where r_{O_2} is the reaction rate, a, b and c are the number of reaction orders for Fe^{2+}, O_2 and H^+, respectively, $C_{Fe^{2+}}$ and C_{H^+} are the instantaneous concentration of Fe^{2+} and H^+, V_{O_2} is the gas flow rate and k the rate constant which is only temperature dependent.

6. Effect of Initial pH

To investigate the effect of the initial pH of O_2 oxidation, the specific experimental conditions are fixed at 60 °C, an O_2 flow rate of 1.2 L/min and a reaction time of 270 min. The effect of differ-

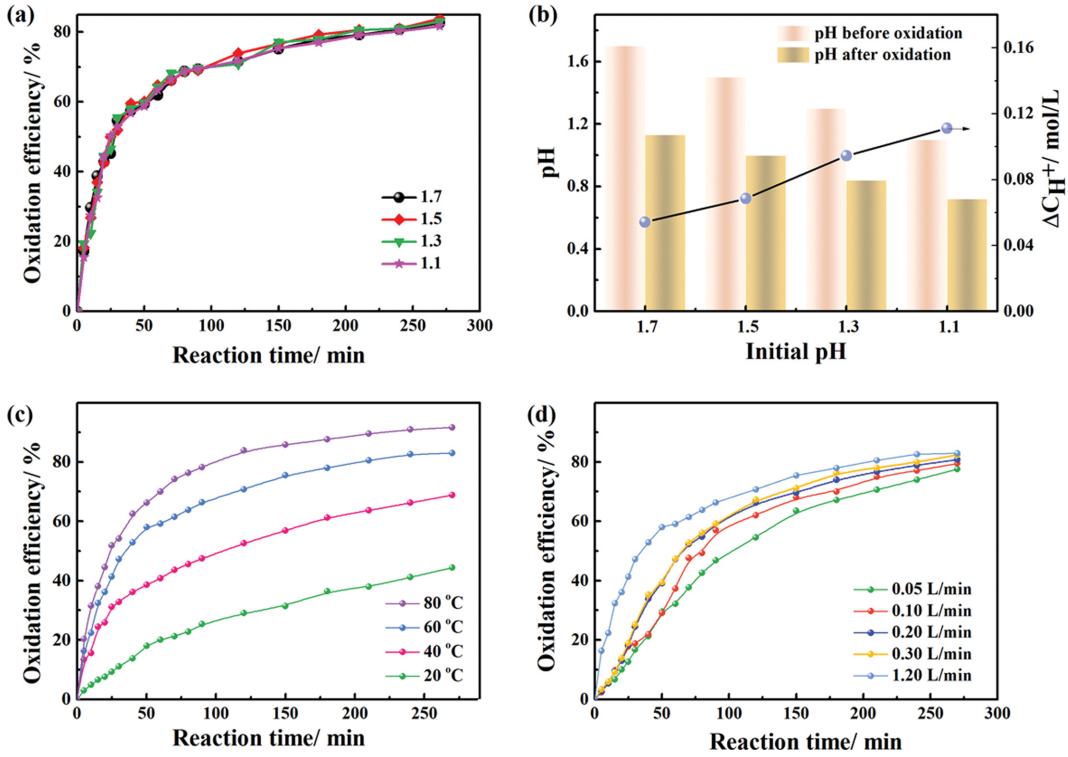

Fig. 6. (a) The oxidation efficiency vs. time at different initial pH values, (b) The relationship between pH value and C_{H^+} after oxidation at different initial pH values, (c) The oxidation efficiency vs. reaction time at different temperatures, (d) The oxidation efficiency vs. reaction time at different O_2 flow rates.

ent initial pH on the oxidation efficiency of Fe^{2+} by O_2 and the effect of pH and C_{H^+} are shown in Fig. 6(a)-(b). According to Fig. 6(a), the oxidation efficiency curves approximately overlap for different initial pH conditions. As seen from Fig. 6(b), the different initial pH of the system leads to a large difference in pH at the end of the reaction, which undergoes a gas-liquid two-phase reaction, ionization and recombination of phosphate groups, complexation of trivalent iron with phosphate groups and other complex reactions, with different pH at any moment in the process. The difference of C_{H^+} generated during the reaction also gradually becomes larger as the initial pH decreases. Combined with the above analysis, it can be concluded that C_{H^+} changes considerably during the reaction, but there is little effect of C_{H^+} on the oxidation of Fe^{2+}.

7. Effect of Temperature

The relationship between oxidation efficiency and reaction time at different temperatures is illustrated in Fig. 6(c). The specific experimental conditions are: an initial pH of 1.3, an O_2 flow rate of 1.2 L/min and a reaction time of 270 min. The results indicate that the oxidation efficiency increases gradually with time and the oxidation rate at the early stage of the reaction is significantly higher than that at the later stage. Meanwhile, the efficiency is positively correlated with the temperature. When the temperature reaches 80 °C, the efficiency can be 91% after 270 min. However, in order to harmonize the timeliness and economy of oxidation behavior, 60 °C is recommended from the viewpoint of the overall process design.

8. Effect of O_2 Flow Rate

Fig. 6(d) exhibits the evolution of Fe^{2+} oxidation efficiency with time at different O_2 flow rates (experimental conditions: an initial pH of 1.3, a reaction time of 270 min and an oxidation temperature of 60 °C). The oxidation efficiency gradually improves with time, and a faster flow rate results in a higher oxidation rate. The oxidation efficiency is 77.6%, 79.5%, 80.8%, 82.3%, and 82.9% after 270 min at O_2 flow rates of 0.05 L/min, 0.10 L/min, 0.20 L/min, 0.30 L/min, and 1.20 L/min, respectively. For the terminal outcome, the efficiency increment is not apparent when it exceeds 0.2 L/min. There may be a threshold for the velocity's influence, which is related to the O_2 solubility in the solution.

9. Kinetic Analysis of O_2 Oxidation

In fact, according to Eq. (4), there should be a certain functional correspondence between r_{O_2} and $C_{Fe^{2+}}$. With data in Fig. 6(c) as the original one, the rate equations for the $C_{Fe^{2+}}$ reaction orders a of 1, 2, 3 and 4 are taken and fitted by least squares method, respectively. The results show that the correlation coefficient of the curve is above 0.99 when a is 2 (Fig. 7(a)), which is considered as the appropriate reaction order. The results of fitting the kinetic data for different flow rates are depicted in Fig. 7(b). The rate equation should be changed to Eq. (5):

$$\left(\frac{1}{C_{Fe^{2+}}}-\frac{1}{C_0}\right)=kV_{O_2}^{b}C_{H^+}^{c}t \tag{5}$$

According to the data in section 3.5.1, it can be concluded that, within the initial pH range of 1.1-1.7, C_{H^+} has little effect on the oxidation reaction, the order of which should be 0, i.e., c=0. The Arrhenius plot of temperature and plot of ln K vs. ln (V_{O_2}) are fitted in Fig. 7(c) and 7(d), respectively. It can be obtained that the apparent activation energy is 34.61 kJ/mol and the reaction order of O_2 flow rate is 5.0. The results reveal that the O_2 oxidation process is controlled by a mixture of chemical reaction and diffusion,

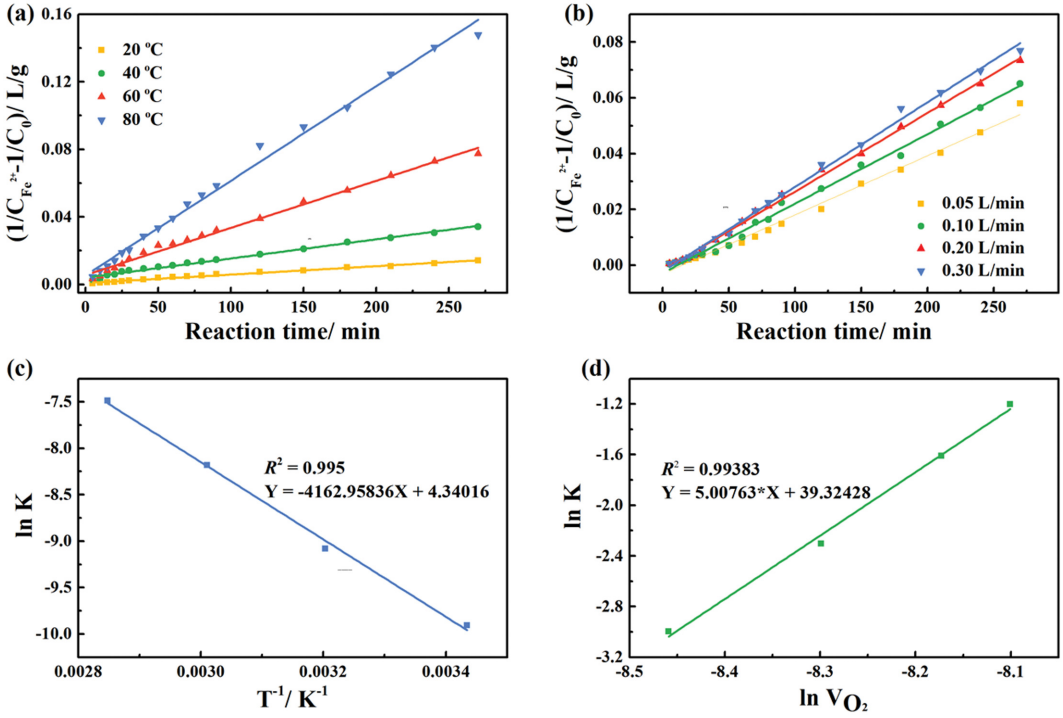

Fig. 7. Plots of ($1/C_{Fe^{2+}}$-$1/C_0$) versus reaction time at (a) different temperatures, (b) oxygen velocities; (c) Arrhenius plot for O_2 oxidizing Fe^{2+} in solutions, (d) Plot of ln K vs. ln V_{O_2}.

and the oxidation rate can be rapidly increased by elevating the temperature of the reactants, increasing the internal mass transfer rate of the reaction system or increasing the concentration of the reactants. The oxidation kinetics equation of spent LFP leaching solution by O_2 is as follows:

$$\left(\frac{1}{C_{Fe^{2+}}}-\frac{1}{C_0}\right)=3.2*10^7*\exp(-34{,}610/RT)*V_{O_2}^5*t \quad (6)$$

10. Kinetics of O_2 and O_3 Mixture Synergistic Oxidation Process

Similar to the pure O_2 oxidation process, a certain rate equation exists for the oxidation process of the mixture of O_2 and O_3:

$$r=\frac{-dC_{Fe^{2+}}}{dt}=k_2C_{Fe^{2+}}^dV_{gas\text{-}mixture}^eC_{H^+}^f \quad (7)$$

where r is the reaction rate, d, e and f are the number of reaction orders for Fe^{2+}, gas mixture and H^+, respectively, $V_{gas\text{-}mixture}$ is the gas flow rate and k_2 is the rate constant.

11. Macrokinetic Data

The effects of initial pH, temperature and gas flow rate are illustrated in Fig. 8(a), 8(c) and 8(d). The pH value before and after oxidation at different initial pH values is shown in Fig. 8(b). The oxidation conditions of the gas mixture are the same as those of the single O_2. The following conclusions could be obtained from Fig. 8: (1) similarly, C_{H^+} hardly exhibits an impact on oxidation efficiency; (2) with the participation of 10% O_3, the oxidation efficiency can exceed 99.9% with a 120 min reaction at 60 °C, which is much faster than 100% O_2 oxidation process; (3) the effects of flow rate on oxidation efficiency are similar to those of pure O_2 oxidation process.

12. Kinetic Analysis of Mixture Synergistic Oxidation

With 10% O_3 in the gas mixture, the oxidation kinetic data at different temperatures are fitted with an empirical equation, Eq. (7), and it is found that the highest correlation coefficient is obtained when the number of reaction order of $C_{Fe^{2+}}$ is 1, as shown in Fig. 9(a). The result of fitting the kinetic data for different flow rates of the gas mixture is depicted in Fig. 9(b).

The Arrhenius plot of temperature and plot of ln K vs. ln $V_{gas\ mixture}$ are fitted in Fig. 9(c)-9(d), respectively. The activation energy of the gas mixture oxidation can be obtained as 28.68 kJ/mol, which is lower than that of pure O_2 oxidation. The number of reaction order of gas mixture flow rate is 0.93. In fact, eliminating the oxidation effect of 90% of the O_2 in the gas mixture with Eq. (6), it can be calculated that the oxidation activation energy of pure O_3 is only 14.27 kJ/mol, which is essentially diffusion controlled, indicating the actual great oxidation capacity of O_3. The oxidation kinetics equation of spent LFP leaching solution by 90% O_2+10% O_3 is as follows:

$$\ln(C_0/C_{Fe^{2+}})=678.58*\exp(-28{,}677/RT)*V_{gas\text{-}mixture}^{0.93}*t \quad (8)$$

13. Evaluation of the Oxidation Methods

For the determination of the optimal oxidation method, two aspects are considered, cost and reaction rate, with oxidation of 1,000 L of solution containing 1 mol/L Fe^{2+} (equivalent to 56 kg Fe^{2+}) as the basis for calculation.

The oxidation costs of different oxidants are compared in Table 1. During the oxidation process, the actual utilization efficiency of H_2O_2 is about 80%, since it is partly decomposed catalytically by Fe^{2+}. The gas oxidizer can be utilized in a gas recovery installation and the solution can be oxidized cyclically. The oxidation efficiency

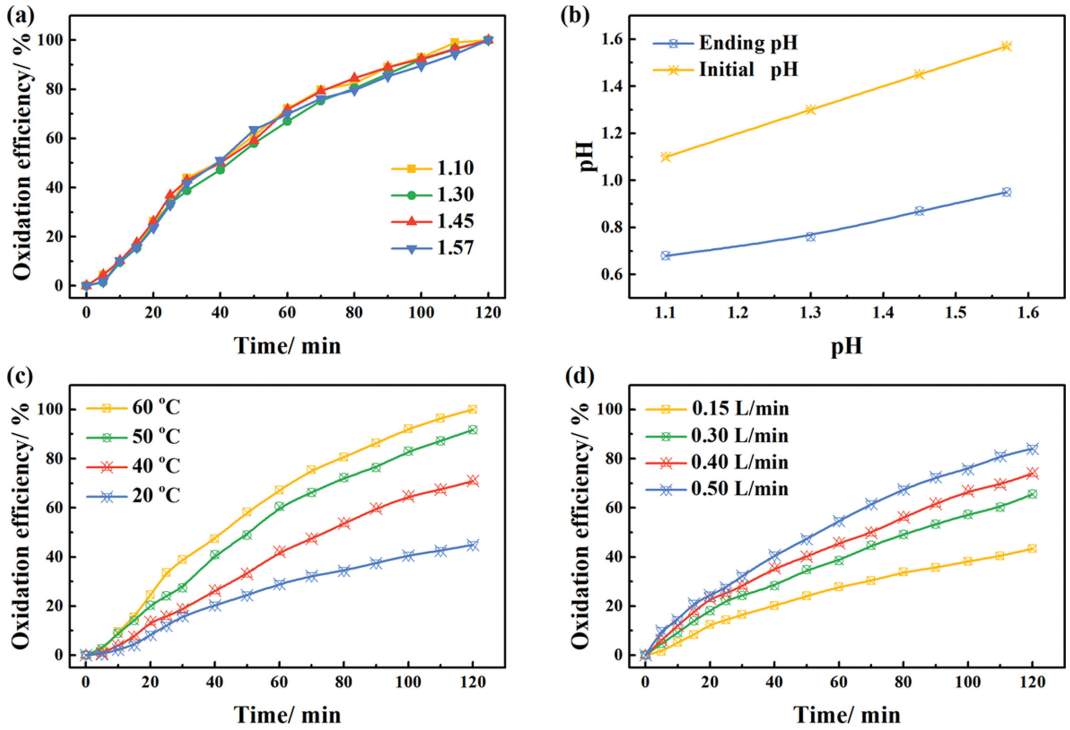

Fig. 8. The oxidation efficiency vs. time at different (a) initial pH values, (c) temperatures, (d) flow rates, (b) pH value before and after oxidation at different initial pH values.

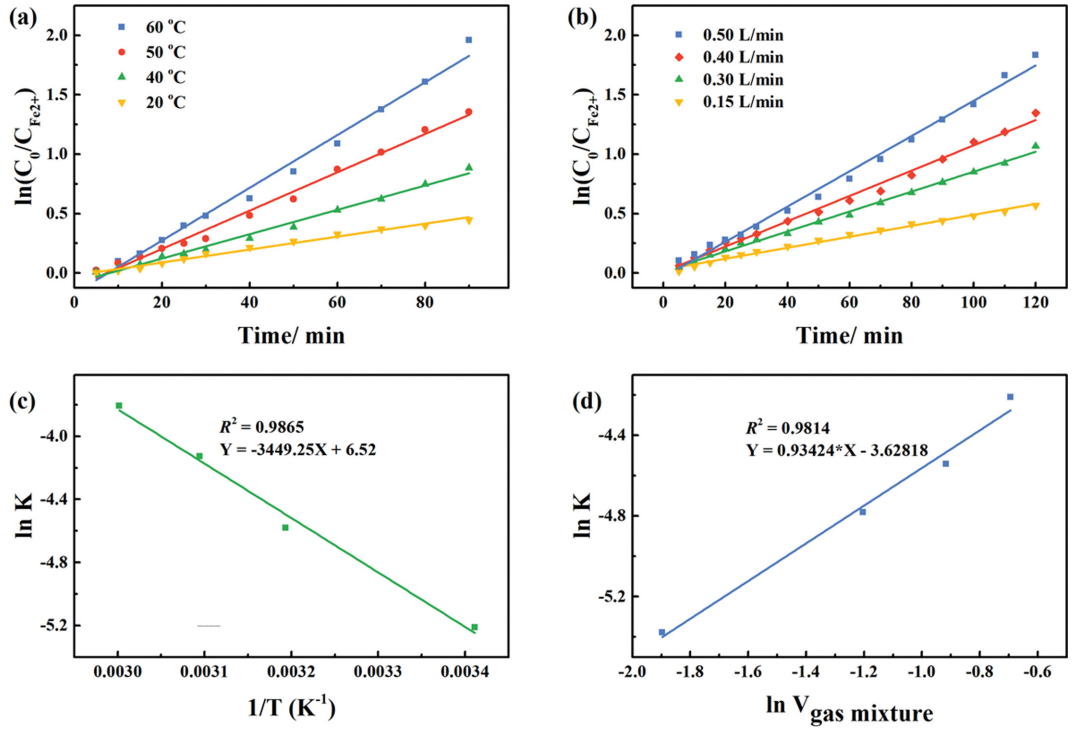

Fig. 9. Plots of $\ln(C_0/C_{Fe^{2+}})$ versus reaction time at different (a) temperatures, (b) gas mixture flow rates; (c) Arrhenius plot for oxidizing Fe^{2+} in solutions (d) Plot of ln K vs. ln $V_{gas\ mixture}$.

Table 1. The comparison of oxidation cost of different oxidants

Oxidants	Price/Yuan/ton	Utilization efficiency	Consumption	Cost/Yuan
H_2O_2	1,550	80%	70.8 kg	109.8
O_2	1,000	100%	5.6 m^3	7.9
Gas mixture ($90\%O_2+10\%O_3$)	1,618	100%	5.4 m^3	12.9

can be considered to be approximately 100% within a fixed oxidation interval. After comparison, the oxidation cost was found to be in the following order: H_2O_2>gas mixture>O_2, where the cost of O_2 is only 7.2% of that of H_2O_2.

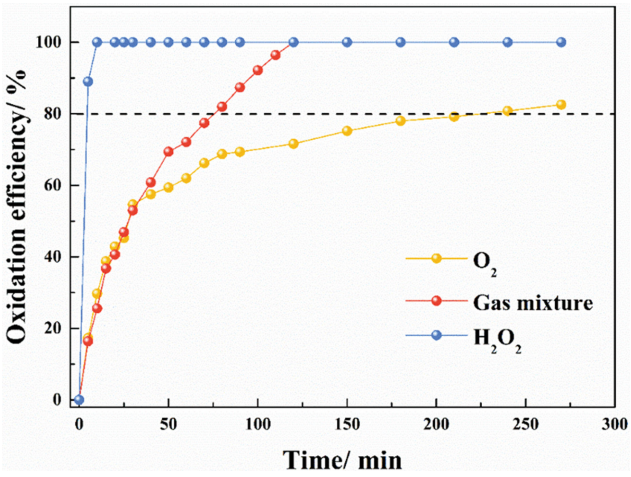

Fig. 10. Oxidation efficiency vs. time of different oxidants.

The oxidation efficiency of different oxidants versus time is compared in Fig. 10, the reaction temperature of which is 60 °C consistently. When H_2O_2 is added into the solution for 10 min, the Fe^{2+} oxidation efficiency can reach 100%; with gas mixture oxidizing the solution, the oxidation efficiency achieves 100% after 120 min; the oxidation efficiency is only about 80% after 240 min with O_2. From the comparison, it is clear that the following relationship exists between the magnitude of the oxidation rate: H_2O_2>gas mixture>O_2.

For the three oxidants mentioned in the text, H_2O_2 has a fast oxidation rate, as well as a high cost; O_2 has a low cost, but a slow oxidation rate; a mixture of O_2 and O_3 costs only 11.7% of that of H_2O_2, while its oxidation rate is much faster than that of O_2. Therefore, for the oxidation of LFP leaching solution, it is considered that it is more advantageous to adopt a gas mixture of 10% O_3 and 90% O_2.

CONCLUSION

Mechanism and process optimization of Fe^{2+} oxidation in phos-

phorus-sulfur mixed acid system by H_2O_2, O_2 and gas mixture were analyzed in comparison. A facile method for efficient synergistic oxidation with a gas mixture of 10% O_3 and 90% O_2 was determined. The main findings were summarized:

(1) The thermodynamic calculation of $\Delta_r G^o$ and $\Delta_r H^o$ results show that all three oxidants have a tendency to oxidize spontaneously and are exothermic.

(2) The main oxidation group of O_3 oxidation process is affected by the acidity, mainly FeO^{2+} at high acidity (C_{H^+}>0.10 mol/L) and $O_2^-\cdot$ at low acidity (C_{H^+}<0.01 mol/L).

(3) After oxidation, a large number of trivalent iron ions complex with the phosphate fraction in the system, mainly forming $Fe_3H_6(PO_4)_4^{3+}$, $FeH_8(PO_4)_4^-$ and $Fe_2HPO_4^{4+}$, release large amounts of hydrogen ions leading to the drop in pH of mixed acid system after oxidation.

(4) The optimum conditions for H_2O_2 oxidation are that the temperature≤65 °C, the rate of H_2O_2 addition≤6 mL/min and the H_2O_2 dosage 1.25 times of the theoretical value. The initial pH of 0.4 to 1.4 has little effect. Finally, the oxidation efficiency can reach 99.6%.

(5) The oxidation of Fe^{2+} in leaching solution by gas mixture and O_2 belongs to the first-order and second-order reactions with activation energies of 28.68 kJ/mol and 34.61 kJ/mol, respectively. They are both controlled by a mixture of chemical reaction and diffusion.

(6) The optimal oxidation method is determined by evaluating both cost and reaction rate; a balance of economy and timeliness can be achieved by employing cyclic oxidation with 10% O_3 and 90% O_2 as the oxidant.

ACKNOWLEDGEMENTS

We gratefully acknowledge support from the Inter-university Cooperation Project of General Undergraduate Colleges and Universities in Liaoning Province (China), the Key Deployment Projects of Chinese Academy of Sciences (No. ZDRW_CN_2020-1), and the Innovation Academy for Green Manufacture, Chinese Academy of Sciences (IAGM-2019-A15).

CONFLICT OF INTEREST

On behalf of all authors, the corresponding author states that there is no conflict of interest.

SUPPORTING INFORMATION

Additional information as noted in the text. This information is available via the Internet at http://www.springer.com/chemistry/journal/11814.

REFERENCES

1. G. Zhou, L. Chen, Y. Chao, X. Li, G. Luo and W. Zhu, *J. Energy Chem.*, **59**, 431 (2021).
2. S. Kim, J. Bang, J. Yoo, Y. Shin, J. Bae, J. Jeong, K. Kim, P. Dong and K. Kwon, *J. Clean. Prod.*, **294**, 126329 (2021).
3. Y.-S. Lee, S.-J. Cho and M. Yoshio, *Korean J. Chem. Eng.*, **23**, 566 (2006).
4. Y. Li, Q. Fu, H. Qin, K. Yang, J. Lv, Q. Zhang, H. Zhang, F. Liu, X. Chen and M. Wang, *Korean J. Chem. Eng.*, **38**, 2113 (2021).
5. Y. Zhang, W. Sun, R. Xu, L. Wang and H. Tang, *J. Clean. Prod.*, **285**, 124905 (2021).
6. Y. Yang, E. G. Okonkwo, G. Huang, S. Xu, W. Sun and Y. He, *Energy Storage Mater.*, **36**, 186 (2021).
7. S. Sakultung, K. Pruksathorn and M. Hunsom, *Korean J. Chem. Eng.*, **24**, 272 (2007).
8. Y. Zhao, X. Yuan, L. Jiang, J. Wen, H. Wang, R. Guan, J. Zhang and G. Zeng, *Chem. Eng. J.*, **383**, 123089 (2020).
9. K. Turcheniuk, D. Bondarev, G. G. Amatucci and G. Yushin, *Mater. Today*, **42**, 57 (2021).
10. H. Ali, H. A. Khan and M. G. Pecht, *J. Energy Storage*, **40**, 102690 (2021).
11. W. B. Hawley and J. Li, *J. Energy Storage*, **25**, 100862 (2019).
12. Y. Wang, N. An, L. Wen, L. Wang, X. Jiang, F. Hou, Y. Yin and J. Liang, *J. Energy Chem.*, **55**, 391 (2021).
13. F. Bella, S. De Luca, L. Fagiolari, D. Versaci, J. Amici, C. Francia and S. Bodoardo, *Nanomaterials*, **11**, 810 (2021).
14. M. Reina, A. Scalia, G. Auxilia, M. Fontana, F. Bella, S. Ferrero and A. Lamberti, *Adv. Sustain. Syst.*, **6**, 2100228 (2022).
15. W. Qiao, B. Jin, W. Xie, M. Shao and M. Wei, *J. Energy Chem.*, **69**, 9 (2022).
16. M. Alidoost, A. Mangini, F. Caldera, A. Anceschi, J. Amici, D. Versaci, L. Fagiolari, F. Trotta, C. Francia, F. Bella and S. Bodoardo, *Chem. Eur. J.*, **28**, e202104201 (2022).
17. P. Mu, H. Zhang, T. Dong, H. Jiang, S. Zhang, C. Wang, J. Li, S. Dong and G. Cui, *Chem. Eng. J.*, **437**, 135032 (2022).
18. M. A. A. M. Abdah, M. Mokhtar, L. T. Khoon, K. Sopian, N. A. Dzulkurnain, A. Ahmad, Y. Sulaiman, F. Bella and M. S. Su'ait, *Energy Rep.*, **7**, 8677 (2021).
19. M. K. Jeon and S.-W. Kim, *Korean J. Chem. Eng.*, In press (2022), https://doi.org/10.1007/s11814-022-1117-0.
20. M. K. Jeon, S.-W. Kim, H.-C. Eun, K. Lee, H. Kim and M. Oh, *Korean J. Chem. Eng.*, **39**, 1472 (2022).
21. P. Meshram, B. D. Pandey and T. R. Mankhand, *Chem. Eng. J.*, **281**, 418 (2015).
22. J. Li, X. Li, Q. Hu, Z. Wang, J. Zheng, L. Wu and L. Zhang, *Hydrometallurgy*, **99**, 7 (2009).
23. Y. Hua, S. Zhou, Y. Huang, X. Liu, H. Ling, X. Zhou, C. Zhang and S. Yang, *J. Power Sources*, **478**, 228753 (2020).
24. M. Chen, X. Ma, B. Chen, R. Arsenault, P. Karlson, N. Simon and Y. Wang, *Joule*, **3**, 2622 (2019).
25. M. Pagliaro and F. Meneguzzo, *Heliyon*, **5**, e01866 (2019).
26. M. Khashij, M. Mehralian and Z. G. Chegini, *Pigm. Resin Technol.*, **49**, 363 (2020).
27. P. Liu, H. Zhang, Y. Feng, F. Yang and J. Zhang, *Chem. Eng. J.*, **240**, 211 (2014).
28. A. Aghaeinejad-Meybodi, A. Ebadi, S. Shafiei, A. Khataee and M. Rostampour, *Environ. Technol.*, **36**, 1477 (2015).
29. Z. Zhao, Z. Liu, H. Wang, W. Dong and W. Wang, *Chemosphere*, **202**, 238 (2018).
30. V. Naddeo, C. S. Uyguner-Demirel, M. Prado, A. Cesaro, V. Belgiorno and F. Ballesteros, *Environ. Technol.*, **36**, 1876 (2015).

31. X. Li, Y. Wang, J. Zhao, H. Wang, B. Wang, J. Huang, S. Deng and G. Yu, *J. Hazard. Mater.*, **300**, 298 (2015).
32. J. Zhang, Y.-L. Zhang, Y.-N. Shi, J. Lin, P. Zhou, W.-Q. Zhang and J.-W. Xu, *Ozone: Sci. Eng.*, **38**, 150 (2016).
33. A. Acosta-Rangel, M. Sánchez-Polo, M. Rozalen, J. Rivera-Utrilla, A. M. S. Polo, M. S. Berber-Mendoza and M. V. López-Ramón, *J. Environ. Manage.*, **255**, 109927 (2020).
34. F. Wang, Z. Lu, L. Yang, Y. Zhang, Q. Tang, Y. Guo, X. Ma and Z. Yang, *Chem. Commun.*, **49**, 6626 (2013).
35. C. Meng, K. Yang, X. Fu and R. Yuan, *ACS Catal.*, **5**, 3760 (2015).
36. T. Kawabata, N. Fujisaki, T. Shishido, K. Nomura, T. Sano and K. Takehira, *J. Mol. Catal. A: Chem.*, **253**, 279 (2006).
37. S.-I. Murahashi, Y. Oda and T. Naota, *Tetrahedron Lett.*, **33**, 7557 (1992).
38. P. K. Saikia, P. P. Sarmah, B. J. Borah, L. Saikia and D. K. Dutta, *J. Mol. Catal. A: Chem.*, **412**, 27 (2016).
39. J. Zang, Y. Ding, L. Yan, T. Wang, Y. Lu and L. Gong, *Catal. Commun.*, **51**, 24 (2014).
40. W. Huang, B. C. Ma, H. Lu, R. Li, L. Wang, K. Landfester and K. A. I. Zhang, *ACS Catal.*, **7**, 5438 (2017).
41. Y.-Z. Chen, Z. U. Wang, H. Wang, J. Lu, S.-H. Yu and H.-L. Jiang, *J. Am. Chem. Soc.*, **139**, 2035 (2017).
42. M. Li, Z. Chen, Z. Wang and Q. Wen, *Chemosphere*, **217**, 223 (2019).
43. B. P. Oruê, A. B. Botelho Junior, J. A. S. Tenório, D. C. R. Espinosa and M. d. P. G. Baltazar, *Ozone: Sci. Eng.*, **43**, 324 (2021).
44. X. Cao, T. a. Zhang, Y. Liu, W. Zhang, S. Li, G. Lv and X. Han, *Nonferrous Met. Sci. Eng.*, **11**, 1 (2020).
45. F. Jiang, B. Qiu and D. Sun, *Chem. Eng. J.*, **370**, 346 (2019).
46. M. Bourgin, B. Beck, M. Boehler, E. Borowska, J. Fleiner, E. Salhi, R. Teichler, U. von Gunten, H. Siegrist and C. S. McArdell, *Water Res.*, **129**, 486 (2018).
47. W. Jia, F. Wang, M. Wang, D. Wang, L. Zheng, A. Ding, B. Liu, X. Liang and H. U. Yu, *S. N. Water Transfers Water Water Sci. Technol.*, **17**, 113 (2019).
48. T. Tao, S. Shaoxian and Y. Jierong, *Chin. J. Power Sources*, **44**, 17 (2020).
49. Y. Wang, Y. Lü, S. Wang and H. Du, *Chin. J. Process Eng.*, **21**, 877 (2021).
50. T. C. Yang and W. C. Neely, *Anal. Chem.*, **58**, 1551 (1986).
51. G. F. Upelaar, R. T. Meijers, R. Hopman and J. C. Kruithof, *Ozone: Sci. Eng.*, **22**, 607 (2000).
52. T. Loegager, J. Holcman, K. Sehested and T. Pedersen, *Inorg. Chem.*, **31**, 3523 (1992).
53. P. Schulte, A. Bayer, F. Kuhn, T. Luy and M. Volkmer, *Ozone: Sci. Eng.*, **17**, 119 (1995).
54. W.-b. Lou, Y. Zhang, Y. Zhang, S.-l. Zheng, P. Sun, X.-j. Wang, J.-z. Li, S. Qiao, Y. Zhang, M. Wenzel and J. J. Weigand, *Trans. Nonferrous Met. Soc. China*, **31**, 817 (2021).
55. W.-b. Lou, Y. Zhang, Y. Zhang, S.-l. Zheng, P. Sun, X.-j. Wang, S. Qiao, J.-z. Li, Y. Zhang, D.-y. Liu, M. Wenzel and J. J. Weigand, *J. Alloys Compd.*, **856**, 158148 (2021).

Supporting Information

A facile method for efficient synergistic oxidation of Fe^{2+} in phosphorus-sulfur mixed acid system with a mixture of oxygen and ozone

Dong-yan Liu*, Wen-bo Lou,***,†, Shi-neng Sun****, Yang Zhang***, Ying Zhang***, and Shi-li Zheng*****

*Normal College, Shenyang University, Shenyang 110044, China
**School of Metallurgy, Northeastern University, Shenyang 110819, China
***National Engineering Research Center of Green Recycling for Strategic Metal Resources, Chinese Academy of Sciences, Institute of Process Engineering, Beijing 100190, China
****Institute of Innovative Science and Technology, Shenyang University, Shenyang 110044, China
(*Received 10 February 2022 • Revised 21 May 2022 • Accepted 12 June 2022*)

Table S1. Oxidation mechanism of O_3

No.	Reactions	Reaction rate constant k
1	$Fe^{2+}+O_3=FeO^{2+}+O_2$	$8.3\times10^5\ M^{-1}\cdot s^{-1}$
2	$Fe^{2+}+FeO^{2+}+2H^+=2Fe^{3+}+H_2O$	$1.4\times10^5\ M^{-1}\cdot s^{-1}$
3	$FeO^{2+}+H_2O=Fe^{3+}+OH\cdot+OH^-$	$1.3\times10^{-2}\ M^{-1}\cdot s^{-1}$
4	$FeO^{2+}+OH\cdot=Fe^{3+}+HO_2^-$	$1.0\times10^{-7}\ M^{-1}\cdot s^{-1}$
5	$FeO^{2+}+H_2O_2=Fe^{3+}+HO_2\cdot+OH^-$	$1.0\times10^4\ M^{-1}\cdot s^{-1}$
6	$FeO^{2+}+HO_2\cdot=Fe^{3+}+O_2+OH^-$	$2.0\times10^6\ M^{-1}\cdot s^{-1}$
7	$2FeO^{2+}\rightarrow(FeOOFe^{4+})+H_2O\rightarrow2Fe^{3+}+OH^-+HO_2^-$	
8	$Fe^{2+}+O_3=Fe^{3+}+O_3^-$	$1.7\times10^5\ M^{-1}\cdot s^{-1}$
9	$O_3^-+H^+=O_2+OH\cdot$	$7\times10^{10}\ M^{-1}\cdot s^{-1}$
10	$Fe^{2+}+OH\cdot=Fe^{3+}+OH^-$	$3\times10^8\ M^{-1}\cdot s^{-1}$
11	$O_3+OH\cdot=HO_2+O_2$	$1.1\times10^8\ M^{-1}\cdot s^{-1}$
12	$O_3+HO_2=OH\cdot+2O_2$	$1.5\times10^9\ M^{-1}\cdot s^{-1}$
13	$HO_2\cdot+H^++Fe^{2+}=H_2O_2+Fe^{3+}$	$1.2\times10^6\ M^{-1}\cdot s^{-1}$
14	$O_2^-\cdot+2H^++Fe^{2+}=H_2O_2+Fe^{3+}$	$1.0\times10^7\ M^{-1}\cdot s^{-1}$
15	$HO_2\cdot+Fe^{3+}=Fe^{2+}+O_2+H^+$	$\leq10^4\ M^{-1}\cdot s^{-1}$
16	$O_2^-\cdot+Fe^{3+}=Fe^{2+}+O_2$	$1.5\times10^8\ M^{-1}\cdot s^{-1}$
17	$Fe^{2+}+H_2O_2=Fe^{3+}+OH\cdot+OH^-$	$67\ M^{-1}\cdot s^{-1}$
18	$FeOH^++H_2O_2=FeOH^{2+}+OH\cdot+OH^-$	$3.8\times10^5\ M^{-1}\cdot s^{-1}$
19	$O_3+OH^-=O_2^-\cdot+HO_2\cdot$	$70\ M^{-1}\cdot s^{-1}$
20	$O_3+HO_2\cdot=HO\cdot+2O_2$	$1.6\times10^9\ M^{-1}\cdot s^{-1}$

Table S2. Composition comparison of leaching solution and simulated solution

Name	Initial pH	Li/g/L	Fe/g/L	Al/g/L	P/g/L
Phosphorus-sulfur mixed acid system	1.30	7.04	56.10	1.43	28.07
A single sulfuric acid system	1.30	7.00	56.21	1.40	0.00